

Received July 28, 2021, accepted August 21, 2021, date of publication August 24, 2021, date of current version September 8, 2021.

Digital Object Identifier 10.1109/ACCESS.2021.3107507

Modeling and Theoretical Analysis of the SERS Enhancement Factor Considering the Electronic Structural Energy

XU YANG¹, ZHEN ZHOU¹, JIA QI¹, SIQI ZHANG², KANGKANG GUO¹, AND SHOUBO ZHAO¹

¹Heilongjiang Province Key Laboratory of Laser Spectroscopy Technology and Application, Harbin University of Science and Technology, Harbin 150080, China

²School of Photoelectric Engineering, Changzhou Institute of Technology, Changzhou 213032, China

Corresponding author: Zhen Zhou (zhzh49@126.com)

This work was supported in part by the National Natural Science Foundation of China under Grant 61801148, and in part by the Scientific Research Project of Harbin University of Science and Technology under Grant LGYC2018JC051.

ABSTRACT The enhancement factor is one of the key parameters characterizing the phenomenon of surface-enhanced Raman scattering. At present, this parameter is described by an empirical formula or a certain single physical mechanism instead of a unified model of the chemical and electromagnetic enhancement mechanisms. It is necessary to integrate the dual enhancement mechanisms of SERS to more accurately obtain the SERS enhancement factor with molecular selectivity. Therefore, we propose a quantitative model for the prediction of the enhancement factor that includes the two main contributions, metal plasmon resonance and electronic structure. Theoretical analysis and verification by experimental results prove that the new predictive enhancement factor (EF) model of electronic structural energy improves the enhancement factor by approximately 10 times and can be used to calculate the enhancement factors of different molecules on the same substrate material, which can provide molecular selectivity and more accurate EF predictions. This paper presents a theoretical model of the SERS enhancement factor that includes the adsorption of the adsorbed molecules and the surface of the substrate, combines the electromagnetic and chemical enhancement mechanisms for surface-enhanced Raman scattering, and provides a deep comprehension of the phenomenon of surface-enhanced Raman scattering.

INDEX TERMS Surface-enhanced Raman scattering, localized surface plasmons, metallic nanoparticles, electromagnetic enhancement, chemical enhancement.

I. INTRODUCTION

Surface-enhanced Raman scattering (SERS) based on the Raman effect of adsorbed molecules is a new spectral detection technique with high efficiency, sensitivity, real time data acquisition and good specificity [1], [2], and it is widely used for molecular identification and characterization, surface treatment of engineering materials, and applications in life science, food safety and other fields [3]–[6]. Experimental research on the preparation of SERS substrate materials has continuously advanced with the development of nanoparticle manufacturing technology [7]–[9], and one result has been more demanding requirements for theoretical SERS research.

In the preparation of SERS substrate materials, researchers have mainly improved substrate nanomaterials to enhance the

Raman signal, thereby improving the accuracy of quantitative spectral analysis [10]–[13]. Metal nanomaterials have always been focuses of SERS substrate preparation research due to their localized surface plasmon resonance (LSPR) characteristics. An Au@AgNP-enhanced substrate to achieve high-throughput recognition of single exosome vesicles was prepared by core-shell technology [14]. A three-dimensional Ag/ZnO/Au structure as a SERS substrate by thermal evaporation, sputtering and other processes was prepared and realized its application in biosensors by detecting λ -DNA molecules [15]. To overcome the limitations of precious metals as substrate materials, some researchers have gradually expanded to nonplasma materials [16], [17]. A label-free, biocompatible, ZnO-based, 3D semiconductor quantum probe for the in vitro diagnosis of cancer was introduced [18]. Although there are many experimental studies on the preparation of SERS substrate materials, the reproducibility of

The associate editor coordinating the review of this manuscript and approving it for publication was Giovanni Angiulli.

the SERS signal produced by the interactions between the substrates and the analytes is poor.

Compared with the progress made in the experimental preparation of SERS substrate materials [19], [20], theoretical research on SERS theory has lagged, mainly because the SERS effect is very complex [21]. Many factors have an impact on the SERS effect such as the surface morphology and surface electronic structure, the interaction of light with rough surfaces, the interaction of light and molecules, the orientations of molecules on surfaces, bonding effects and so on [22]–[24]. The enhancement mechanisms of the SERS effect are mainly divided into electromagnetic (EM) and chemical (CM) contributions [25], [26]. The former a physical enhancement mechanism, mainly considers the enhancement of the electric field by the microstructure of the reinforced substrate, and the latter a chemical enhancement mechanism, mainly considers the chemical interactions between the molecule of interest and the reinforced substrate [27]–[29].

The SERS enhancement factor (EF) is the most intuitive parameter for evaluating the enhancement of SERS, and many empirical formulas have been established to evaluate it such as the single molecule, orientation-averaged single molecule, and analytical enhancement factors [30]–[33]. Because the determination of an empirical formula requires information including the concentration and molecular weight, an empirical formula cannot predict the enhancement effect. In addition, various empirical formulas predict different values of the enhancement effect for the same molecule on the same base material because of the lack of strict theoretical basis. At present, theoretical calculations of the SERS enhancement factor mainly follow the assumption that the EF is proportional to the 4th power of the electromagnetic enhancement [34]. The calculation and verification of electromagnetic enhancement factor theory was enriched by the development of plasma resonance technology. For example, the influence of the surface selection rules on the SERS enhancement factor at the hot spot received special consideration, and an additional theory of depolarization was proposed by the E. C. L. Ru team on the basis of the SERS electromagnetic enhancement factor [35]. According to electromagnetic theory, the electromagnetic gain of SERS is related to the amplitude and resonance bandwidth of the local field, in addition the average localization factor at the same frequency is consistent with the average Purcell radiation factor [36]. However, the above electromagnetic enhancement factor theory could not provide enough information to explain the repeatability of substrates and considered only the characteristics of metal nanoparticles; as a consequence, theoretical calculations of electromagnetic enhancement differed from actual measured Raman enhancement signals. EM and CM enhancement mechanisms are present at the same time, and only one mechanism (electromagnetic or chemical enhancement) could not explain all SERS phenomena. Therefore, it is necessary to establish a unified theoretical model of electromagnetic and chemical enhancement mechanisms to obtain

a theoretical enhancement factor that is more appropriate for experimental applications and can fully explain the SERS enhancement phenomenon.

Based on the above discussion, this paper establishes a theoretical model for the calculation of SERS enhancement factors of metal nanoparticles based on the local surface plasma effect and electronic structure theory, analyzes the effects of the properties, size and shape of metal nanoparticles on SERS enhancement, and considers the influence of the adsorption between the molecule to be tested and the substrate material on the SERS enhancement. We unify the electromagnetic and chemical mechanisms of the SERS effect and establish a theoretical model to predict the SERS enhancement effect. This not only provides theoretical guidance for surface enhanced spectroscopy but also provides a possible approach for the clear analysis of microscopic structural information and macroscopic material properties in material science.

II. SERS ENHANCEMENT FACTOR MODEL WITH DUAL MECHANISMS

According to the theory of classical mechanics, the light intensity of Raman scattering is proportional to the square of the induced electric dipole moment P . Under the action of an incident photoelectric field, the induced electric dipole moment P is:

$$P = \alpha E \quad (1)$$

where α is the molecular polarizability and E is the electric field strength.

The above formula shows that increasing the molecular polarizability or increasing the electric field strength can increase the electric dipole moment, thereby realizing the enhancement of the Raman scattered light intensity. Therefore, the enhancement mechanism of SERS consists of two categories, namely, EM enhancement and CM enhancement.

There are two main sources of the electromagnetic field enhancement mechanism. First, local electric field enhancement [37] is realized by local surface plasmon resonance, and the local field enhancement factor M_{Loc} is:

$$M_{\text{Loc}}(\omega_0, r_m) = \left| \frac{E_{\text{Loc}}(\omega_0, r_m)}{E_0(\omega_0, r_m)} \right|^2 \quad (2)$$

where $E_{\text{Loc}}(\omega_0, r_m)$ is the local electric field strength at position r_m of the molecule, E_0 is the incident light field, and ω_0 is the incident wave frequency.

Second, similar to modified spontaneous emission, the radiated enhancement factor M_{Rad} is usually approximated by the optical reciprocity theorem:

$$M_{\text{Rad}}(\omega_R, r_m) = \left| \frac{E_{\text{Loc}}(\omega_R, r_m)}{E_0(\omega_R, r_m)} \right|^2 \quad (3)$$

where $E_{\text{Loc}}(\omega_R, r_m)$ is the plane wave light field $E_0(\omega_R, r_m)$ in the local field generated at the Raman scattering frequency ω_R .

The enhancement of the entire SERS at r_m can be approximated as:

$$M_{EM} = M_{loc}(\omega_0, r_m) M_{Rad}(\omega_R, r_m) \quad (4)$$

When the frequency of Raman scattered light is very close to the frequency of incident light, equation (4) is simplified to:

$$M_{EM} = \left| \frac{E_{Loc}(\omega_0, r_m)}{E_0(\omega_0, r_m)} \right|^2 \cdot \left| \frac{E_{Loc}(\omega_R, r_m)}{E_0(\omega_R, r_m)} \right|^2 \approx \left| \frac{E_{Loc}(\omega_0, r_m)}{E_0(\omega_0, r_m)} \right|^4 \quad (5)$$

where M_{EM} is the electromagnetic enhancement factor. Equation (5) is the $|E|^4$ approximation hypothesis of the SERS enhancement factor [38].

The chemical enhancement mechanism mainly considers the interaction between the metal nanosurface and the molecule to be tested, which is caused by the change in electronic structure. When free molecules adsorb on a metal surface, the electronic structure changes. The electronic structure can be solved by density functional theory (DFT), which uses the laws of quantum mechanics to address the electrical properties of solids. The Kohn-Sham method for DFT reduces the difficulty of solving a multielectron problem to that of a noninteracting electron moving in an effective potential field [39] and gives the specific electronic structure energy E_s expression:

$$E_s = \sum_i^n f_i \varepsilon_i - \frac{1}{2} \iint \frac{\rho(\vec{r})\rho(\vec{r}')}{|\vec{r} - \vec{r}'|} d\vec{r} d\vec{r}' + E_{XC}[\rho(\vec{r})] - \int \rho(\vec{r}) V_{XC}(\vec{r}) d\vec{r} \quad (6)$$

where f_i is the orbital occupancy number, ε_i is the electron orbital energy, $\rho(\vec{r})$ is the electron density of the system, \vec{r} is the electron coordinate, $E_{XC}[\rho(\vec{r})]$ is the interaction energy between electrons, and $V_{XC}(\vec{r})$ is the functional derivative of the exchange correlation quantity.

We define the chemical enhancement factor M_{CM} as the increase in electronic structural energy caused by the interaction between the test molecule and substrate material:

$$M_{CM} = \left| \frac{E_{tot}}{E_{mol}} \right| \quad (7)$$

where E_{tot} is the total electronic structural energy of the equilibrium adsorption system, and E_{mol} is the electronic structural energy of the molecule to be measured.

In summary, a priori, the two enhancement mechanisms have nothing in common and are independent of each other. However, both of mechanisms can lead to the enhancement of SERS. The expected value of the SERS effect could be equivalent to the product of the two effects. Therefore, the SERS enhancement factor model can be described as:

$$EF = M_{EM} M_{CM} = \left| \frac{E_{Loc}}{E_0} \right|^4 \cdot \left| \frac{E_{tot}}{E_{mol}} \right| \quad (8)$$

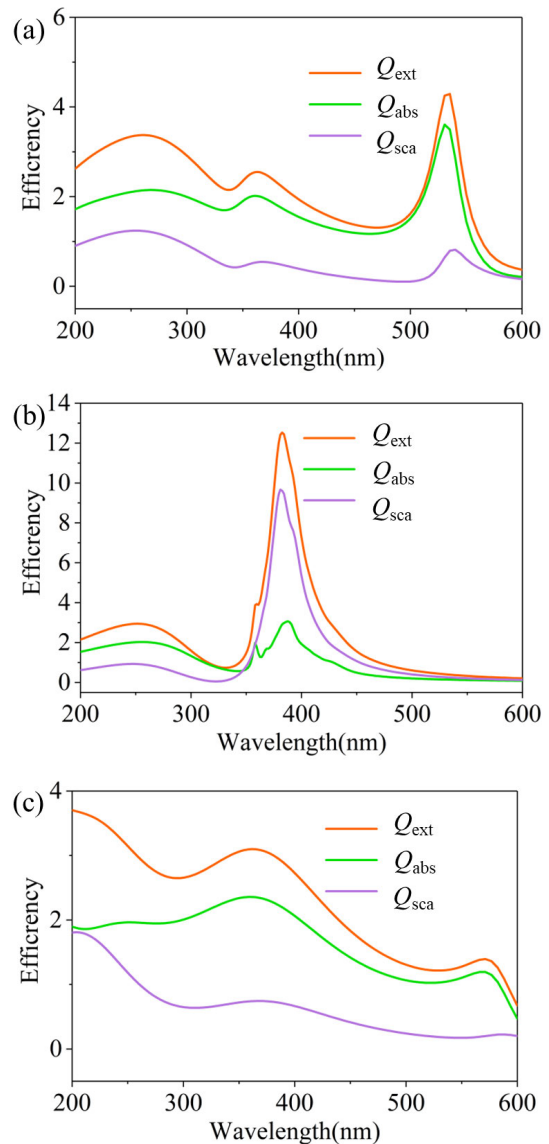


FIGURE 1. Scattering, extinction and absorption spectra of Au, Ag and Cu nanospheres with $r = 40$ nm: (a) Au (b) Ag and (c) Cu.

III. ANALYSIS AND DISCUSSION

A. A THEORETICAL ANALYSIS OF ELECTROMAGNETIC ENHANCEMENT

The main theoretical basis of the electromagnetic enhancement mechanism is that metal base materials have a strong LSPR which is related to the properties of metal base materials and the dimensions and shape of metal nanoparticles. Coin group metals such as Au, Ag, and Cu can generate obvious LSPR effects. The variations in the scattering efficiency, extinction efficiency and absorption efficiency of Au, Ag and Cu nanospheres are analyzed for a radius of 40 nm and shown in Figure 1. The Au, Ag and Cu nanospheres have obvious resonance peaks for scattering, extinction and absorption in different wavelength bands. The resonance peak wave band of the Au nanospheres is more biased toward the direction of

red light than is the case for the Ag and Cu nanospheres. The extinction coefficient of the Ag nanospheres is approximately 3 times that of the Au and Cu nanospheres of the same size, and the scattering coefficient of the Ag nanospheres is approximately 5 times that of the Au and Cu nanospheres indicating that the Ag nanospheres have stronger extinction and scattering abilities than Cu and Au at the same radius.

In terms of LSPR dimensional effects, the electric field intensities of 10 spherical Ag nanoparticles were calculated for a size range from 5 to 55 nm and a spacing of 5 nm, as shown in Figure 2. As the radius increases, the electric field intensity of Ag nanoparticles first increases and then decreases. When the Ag nanosphere radius is 15 nm, the electric field intensity reaches its maximum, and the electric field enhancement factor is 40.614. The internal electric field of the particles decreases, reducing the resonance frequency and the electric field strength, when the size is greater than 30 nm.

The LSPR effects of Ag nanoparticles with different geometric shapes on the surface, such as triangular, quadrilateral, hexagonal, and five-pointed star, are considered. The local electric field distributions of Ag nanoparticles of different shapes in the X-Y plane are calculated separately, as shown in Figure 3. The electric field signal is significantly enhanced at the tip of the particle edge. When the incident wavelength is 514 nm, the maximum electric field enhancement factors of Ag nanoparticles are 54.573, 6.391, 14.195 and 16.777 with triangular, quadrilateral, hexagonal and five-pointed star shapes, respectively. Among them, the triangle has the largest electric field enhancement factor, which is inconsistent with the rule that the more particle vertices there are, the more complex the spectrum and the stronger the electric field enhancement effect. However, the other three shapes of nanoparticles conform to this rule.

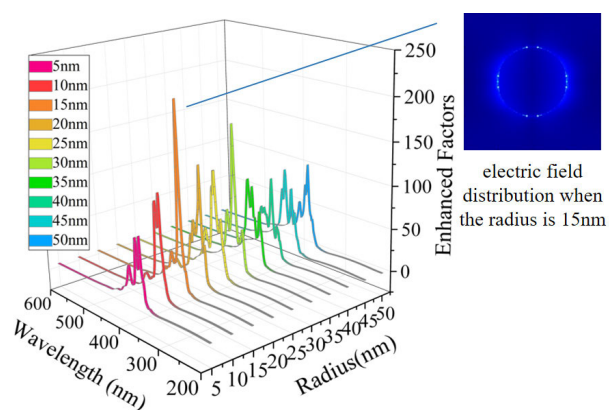


FIGURE 2. The electric field intensity changes of Ag nanospheres for different radii and the electric field distribution when the radius is 15 nm.

B. THEORETICAL ANALYSIS OF CHEMICAL ENHANCEMENT

Probe molecules are commonly used in SERS analysis to measure the enhancement effect. Pyridine (Py) is one of the most important SERS probe molecules [40], so we studied

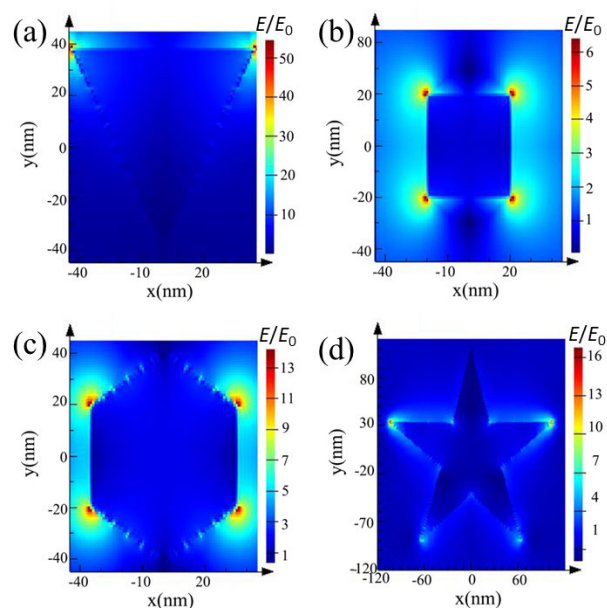


FIGURE 3. FDTD electromagnetic field simulation results in the X, Y-plane. (a) Triangle; (b) Quadrilateral; (c) Hexagon; (d) Pentagon.

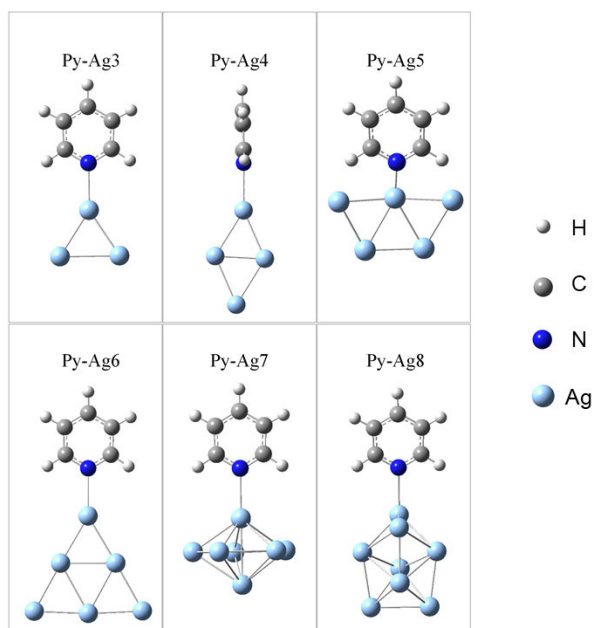
the Raman enhancement effect after it interacts with metal nanoparticles. The Py-Agn ($n=3, 4, 5, 6, 7, 8$) structure was established by the metal cluster model, and the equilibrium structure was calculated by the hybrid density functional B3LYP method. For C, H, and N, the all-electron basis set 6-311+G(d, p) was adopted, and for the Ag atom, the LANL2DZ pseudopotential basis set was used. The optimized Py-Agn configuration is shown in Figure 4. When pyridine and metal nanoparticles adsorb, nitrogen atoms adsorb with silver atoms in metal clusters, producing N-Ag chemical bonds rather than binding with other atoms.

The changes in the N-Ag bond distance, energy and energy level of the Py-Agn complex are shown in Table 1. The adsorption distance does not vary with the size of the metal clusters, and the N-Ag bond lengths of the six configurations are similar. With the increase in the number of metal clusters, the adsorption energy of the system at equilibrium decreases, and the adsorption capacity and stability of the system increase. The number of metal cluster atoms affects the orbital system of the composite molecule. When the number of atoms is even, Py-Agn is a closed-shell system; when it is singular, Py-Agn is an open-shell system. In the SERS system, the direction of charge transfer is determined by the relative position of the front orbital of the adsorbed molecule and the Fermi level of the metal. Taking Py-Ag₄ as an example, the HOMO orbital energy level is 3.952 eV, the LUMO orbital energy level is 2.584 eV, and the Fermi energy level of Ag₄ is 3.94 eV. The charge transfer direction for Py-Ag₄ adsorbed on the Ag surface should be from molecule to metal because the HOMO orbital of Py-Ag₄ is close to the Fermi level of Ag₄.

We calculated the SERS spectra of the optimized structures of the six Py-Agn complexes and compared them with the

TABLE 1. N-Ag bond distances, energies and energy levels of Py-Agn complexes.

Mode	Bond Distances (N-Ag) (Å)	E (Hartree)	Energy level (eV)	
			HOMO	LUMO
Py-Ag3	2.334	-685.640	-3.420	-2.120
Py-Ag4	2.504	-831.444	-3.952	-2.584
Py-Ag5	2.445	-977.256	-4.032	-1.880
Py-Ag6	2.412	-1123.091	-4.810	-2.019
Py-Ag7	2.443	-1268.881	-3.720	-2.053
Py-Ag8	2.445	-1414.709	-4.656	-2.098

**FIGURE 4.** Modeling structures and optimized geometries of Py-Agn.

intensities of the Raman peaks of the pyridine molecule. As shown in Figure 5, the six configurations with adsorbed silver nanoparticles all enhanced the Raman spectrum of the pyridine molecule. In addition to the two main peaks that are consistent with the experimental peaks [41] measured at 1006 and 1035 cm^{-1} , the Py-Agn complexes also have two strong peaks at 1238 and 1634 cm^{-1} . The peak at 1238 cm^{-1} refers to the in-plane bending vibration $\rho(\text{C-H})$ of the C-H bond, and the peak at 1634 cm^{-1} refers to the symmetric stretching vibration ν_s of the benzene ring. With the increase in the number of silver atoms in the metal clusters, the $\rho(\text{C-H})$ vibration mode weakens and the ν_s vibration mode strengthens, indicating that chemical adsorption has little effect on the vibration of molecules on the Benzene ring and mainly affects the vibrational mode of the adsorption site.

C. VALIDATION AND ANALYSIS OF THE THEORETICAL MODEL OF THE SERS ENHANCEMENT FACTOR

We selected three sets experimental results for SERS substrate preparation to verify the accuracy of our theoretical

model of the SERS enhancement factor. First, we calculated the enhancement effect of the electromagnetic field based on the substrate material prepared in the experiment. Considering the influence of the nanoparticle gap on the electric field enhancement effect, we designed triangular prism Ag nanoparticles with a side length of 30 nm and a thickness of 10 nm by referring to the morphology of the prepared particles in an experiment [42]–[44]. Cubic Ag nanoparticles with a length of 110 nm and a thickness of 110 nm and hexagonal Ag nanoplate particles with a side length of 85 nm and a thickness of 25 nm were also used. The effect of multiparticle electric field enhancement is shown in Figure 6. The localized electric field intensities of normalized triangular prism, cubic, and hexagonal Ag nanoparticles are 8.008, 12.028, and 47.429, respectively.

Second, we analyzed the electronic structural energy and Raman enhancement effect when the molecule of interest interacts with the metal cluster. Based on the molecules used in the experiment, 4-mercaptobenzoic acid, crystal violet and methylene blue, density functional theory calculations were performed on 4-MBA, CV and MB respectively, and for C, H, O, N, S, the all-electronic basis set 6-311+G(d,p) was used. For Ag atoms, the LANL2DZ pseudopotential basis set was used. The configuration of 4-MBA-Ag3 is shown in Figure 7(a). After optimization, 4-MBA molecules mainly interact with Ag clusters through S atoms, and the adsorption energy E_{ads} is 2.748 eV, resulting in a strong Ag-S bond. Figure 7(d) shows the Raman peaks of 4-MBA and 4-MBA-Ag3. The strongest SERS peak of 4-MBA-Ag3 appeared at 1633 cm^{-1} because of the coupling of the stretching vibration of the carbon-carbon bond on the benzene ring in 4-MBA and the in-plane rocking vibration of the hydrocarbon, which is consistent with the characteristic peak measured in the experiment.

Because there are many adsorption sites for CV and MB molecules, we consider only one adsorption situation here. The configuration of CV-Ag14 is shown in Figure 7(b). After optimization, CV molecules interact with Ag clusters through N atoms, and the adsorption energy E_{ads} is 2.353 eV, resulting in a strong Ag-N bond. Figure 7(e) shows the Raman peaks of CV and CV-Ag14. The strongest SERS peak of CV-Ag14 appears at 1652 cm^{-1} , which is attributed to the coupling of the torsional motion of the carbon-carbon bond

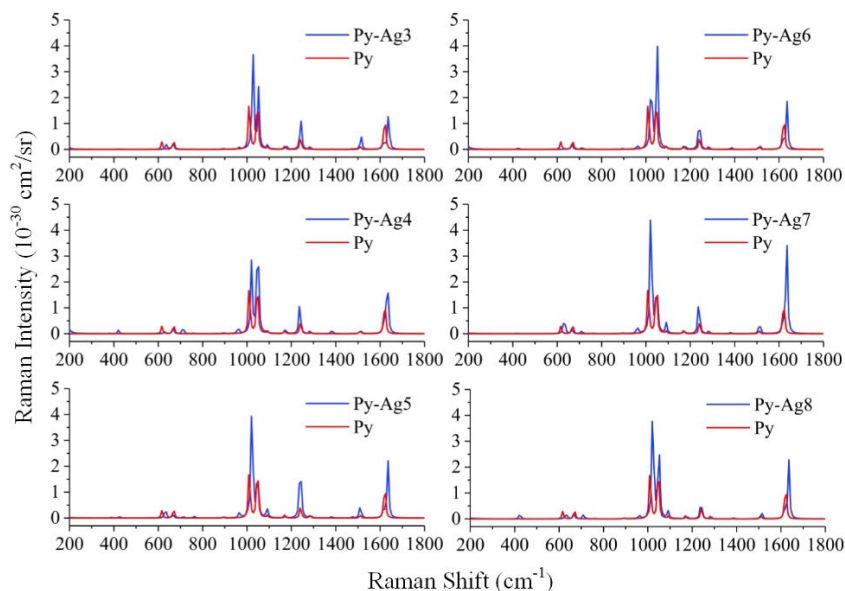


FIGURE 5. Simulated Raman spectra of Py-Agn complexes calculated with B3LYP.

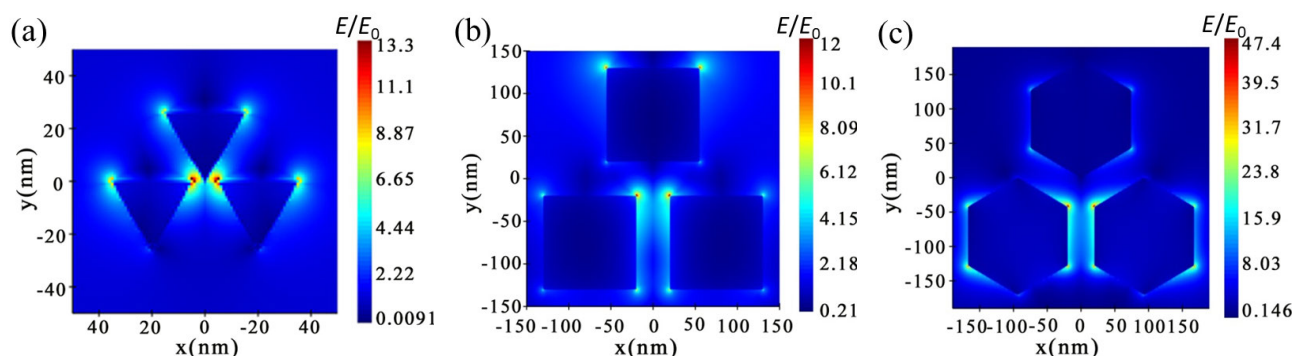


FIGURE 6. Electric field distribution in the X, Y-plane for various Ag nanoparticles. (a) Triangular; (b) Cubic; (c) Hexagonal.

on the benzene ring and the stretching vibration of the carbon-nitrogen bond in the CV.

The configuration of MB-Ag13 is shown in Figure 7(c). After optimization, the N atoms and S atoms on the aromatic ring of the MB molecule interact with the Ag clusters, and the adsorption energy E_{ads} is 0.947 eV. Figure 7(f) shows the Raman peaks of MB and MB-Ag13. Since both N and S adsorb with Ag clusters, the enhancement effect is more significant. MB Raman characteristic peaks appear at 460 and 1649 cm^{-1} , but the strongest peak is at 1380 cm^{-1} , which is considered to be due to Ag. The coupling of the benzene ring carbon-carbon, hydrocarbon and carbon-sulfur bond bending vibrations is caused by clusters.

Table 2 shows the enhancement factors calculated by the empirical formula in the experiments, the theoretical formula (the fourth power of the electromagnetic enhancement), and the new model developed in this paper. The comparison of the calculated results based on different experiments and

different enhancement factors shows that the enhancement factor calculated with the new model in this paper is approximately 10 times higher than the electromagnetic enhancement (4th power) factor, which is in line with the general effect of the chemical enhancement mechanism. This makes our calculated enhancement factor closer to the real results obtained in the experiments. To highlight the molecular selectivity of our theoretical model, we take the base material established experimentally [42] as an example and calculate the enhancement factor produced when it interacts with pyridine molecules, which can be different from 4-MBA molecules. However, the 4th power theoretical model of electromagnetic enhancement is limited by the nonselectivity of the EM mechanism, so the model cannot differentiate the enhancement effect for different molecules adsorbed on the same substrate. The above analysis confirmed that our theoretical model can make selective predictions of the enhancement of SERS. Verification by a variety of test molecules and

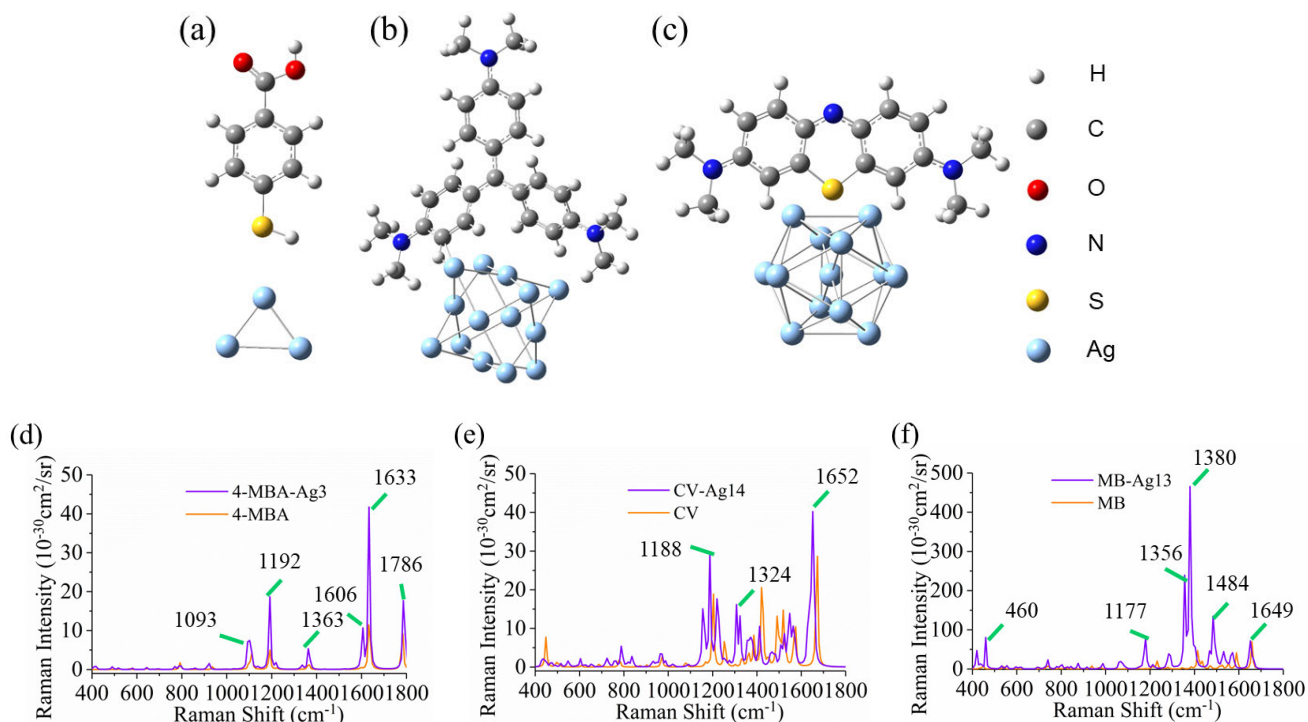
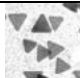
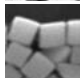
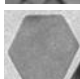


FIGURE 7. (a) Optimized adsorption configuration for 4-MBA-Ag3; (b) Optimized adsorption configuration for CV-Ag14; (c) Optimized adsorption configuration for MB-Ag13; (d) Raman spectra of 4-MBA and 4-MBA-Ag3; (e) Raman spectra of CV and CV-Ag14; (f) Raman spectra of MB and MB-Ag13.

TABLE 2. Enhancement factor comparison.

Experimental Data Source	Nanoparticle Morphology	Empirical Formula $EF' = \frac{I_{SERS} \times C_R}{I_R \times C_{SERS}}$	Theoretical Formula $EF'' = E ^4$	New Model $EF = M_{EM} M_{CM}$
[42]		3.94×10^5	3.13×10^4	8.64×10^4 (Py) 4.80×10^5 (4-MBA)
[43]		5.06×10^7	1.20×10^5	3.22×10^5 (CV)
[44]		1.21×10^9	5.06×10^7	1.26×10^8 (MB)

substrate materials proved that the model is suitable for the analysis of any substrate material and adsorbate and has a certain universality.

IV. CONCLUSION

This paper introduces electronic structural energy to revise the theoretical model of the SERS enhancement factor by combining the EM and CM mechanisms with consideration of the chemical interaction between an adsorbed molecule and substrate material. In terms of metal LSPR characteristics, Ag nanoparticles possess stronger scattering properties than other nanoparticles. The electric field intensity first increases and then decreases with increasing metal nanoparticle size. It is not the case that the more complex the shape

of the metal nanoparticle is, the stronger the electric field intensity. In the quantum chemical analysis of molecule-metal cluster configurations, adsorption and Raman performance are related to the size of the cluster and adsorption energy, and the Raman peak is enhanced by the increase in the number of metal clusters. When different molecules interact with the same metal clusters, the SERS enhancement effect depends on which atoms are bound to the adsorption sites. Finally, through verification and analysis of experimental results, the enhancement factor calculated by our proposed model is increased by approximately 10 times, reflecting the contribution of chemical enhancement, which is more consistent with the actual SERS enhancement effect. In addition, the enhancement factors of different molecules on the same

substrate material were calculated, and selective molecular predictions of the enhancement effect of SERS were realized. The prediction of the SERS enhancement effect was obtained by calculating enhancement factors, which can be used to guide the preparation of SERS substrate materials; this is of great significance for accurately describing surface spectroscopy images and realizing quantitative analyses. Future studies will be extended to SERS-enhanced analyses of transition metals, with potentially great application value in the unified interpretation of SERS CMs and EMs

REFERENCES

- [1] H. Sun, M. Yao, Y. Song, L. Zhu, J. Dong, R. Liu, P. Li, B. Zhao, and B. Liu, "Pressure-induced SERS enhancement in a MoS₂/Au/R6G system by a two-step charge transfer process," *Nanoscale*, vol. 11, no. 44, pp. 21493–21501, 2019.
- [2] H. Kearns, R. Goodacre, L. E. Jamieson, D. Graham, and K. Faulds, "SERS detection of multiple antimicrobial-resistant pathogens using nanosensors," *Anal. Chem.*, vol. 89, no. 23, pp. 12666–12673, Dec. 2017.
- [3] V. Sharma and V. Krishnan, "Fabrication of highly sensitive biomimetic SERS substrates for detection of herbicides in trace concentration," *Sens. Actuators B, Chem.*, vol. 262, pp. 710–719, Jun. 2018.
- [4] G. Demirel, R. L. M. Gieseck, R. Ozdemir, S. Kahmann, M. A. Loi, G. C. Schatz, A. Facchetti, and H. Usta, "Molecular engineering of organic semiconductors enables noble metal-comparable SERS enhancement and sensitivity," *Nature Commun.*, vol. 10, no. 1, pp. 1–9, Dec. 2019.
- [5] V. Moisoiu, A. Socaciu, A. Stefanu, S. Iancu, I. Boros, C. Alecsa, C. Rachieriu, A. Chiorean, D. Eniu, N. Leopold, C. Socaciu, and D. Eniu, "Breast cancer diagnosis by surface-enhanced Raman scattering (SERS) of urine," *Appl. Sci.*, vol. 9, no. 4, p. 806, Feb. 2019, doi: 10.3390/app9040806.
- [6] K. Xu, R. Zhou, K. Takei, and M. Hong, "Toward flexible surface-enhanced Raman scattering (SERS) sensors for point-of-care diagnostics," *Adv. Sci.*, vol. 6, no. 16, Aug. 2019, Art. no. 1900925, doi: 10.1002/advs.201900925.
- [7] C. Kuttner, R. P. M. Höller, M. Quintanilla, M. J. Schnepf, M. Dulle, A. Fery, and L. M. Liz-Marzán, "SERS and plasmonic heating efficiency from anisotropic core/satellite superstructures," *Nanoscale*, vol. 11, no. 38, pp. 17655–17663, 2019.
- [8] J. L. Weyher, B. Bartosewicz, I. Dziecielewski, J. Krajczewski, B. Jankiewicz, G. Nowak, and A. Kudelski, "Relationship between the nano-structure of GaN surfaces and SERS efficiency: Chasing hot-spots," *Appl. Surf. Sci.*, vol. 466, pp. 554–561, Feb. 2019.
- [9] A. K. Nair, K. B. Bhavitha, S. Perumbilavil, P. Sankar, D. Rouxel, M. S. Kala, S. Thomas, and N. Kalarikkal, "Multifunctional nitrogen sulfur co-doped reduced graphene oxide—Ag nano hybrids (sphere, cube and wire) for nonlinear optical and SERS applications," *Carbon*, vol. 132, pp. 380–393, Jun. 2018.
- [10] J. Li, H. Yan, X. Tan, Z. Lu, and H. Han, "Cauliflower-inspired 3D SERS substrate for multiple mycotoxins detection," *Anal. Chem.*, vol. 91, no. 6, pp. 3885–3892, Mar. 2019.
- [11] Z. Wang, C. Zheng, P. Zhang, Z. Huang, C. Zhu, X. Wang, X. Hu, and J. Yan, "A split-type structure of Ag nanoparticles and Al₂O₃@Ag@Si nanocone arrays: An ingenious strategy for SERS-based detection," *Nanoscale*, vol. 12, no. 7, pp. 4359–4365, 2020.
- [12] Y. Li, L. Feng, J. Li, X. Li, J. Chen, L. Wang, D. Qi, X. Liu, and G. Shi, "Fabrication of an insect-like compound-eye SERS substrate with 3D Ag nano-bowls and its application in optical sensor," *Sens. Actuators B, Chem.*, vol. 330, Mar. 2021, Art. no. 129357.
- [13] Y. Kalachyova, M. Erzina, P. Postnikov, V. Svorcik, and O. Lyutakov, "Flexible SERS substrate for portable Raman analysis of biosamples," *Appl. Surf. Sci.*, vol. 458, pp. 95–99, Nov. 2018.
- [14] J. C. Fraire, S. Stremersch, D. Bouckaert, T. Monteyne, T. De Beer, P. Wuytens, R. De Rycke, A. G. Skirtach, K. Raemdonck, S. De Smedt, and K. Braeckmans, "Improved label-free identification of individual exosome-like vesicles with Au@Ag nanoparticles as SERS substrate," *ACS Appl. Mater. Interfaces*, vol. 11, no. 43, pp. 39424–39435, Oct. 2019, doi: 10.1021/acsami.9b11473.
- [15] A. K. Pal, S. Pagal, K. Prashanth, G. K. Chandra, S. Umopathy, and D. B. Mohan, "Ag/ZnO/Au 3D hybrid structured reusable SERS substrate as highly sensitive platform for DNA detection," *Sens. Actuators B, Chem.*, vol. 279, pp. 157–169, Jan. 2019.
- [16] L. B. Wang, C. Li, Y. Luo, and Z. Jiang, "Preparation of highly catalytic N-doped carbon dots and their application in SERS sulfate sensing," *Materials*, vol. 11, no. 9, pp. 1655, 2018, doi: 10.3390/ma11091655.
- [17] Y. Zhou, A. E. Hartemink, Z. Shi, Z. Liang, and Y. Lu, "Land use and climate change effects on soil organic carbon in north and northeast China," *Sci. Total Environ.*, vol. 647, pp. 1230–1238, Jan. 2019, doi: 10.1016/j.scitotenv.2018.08.016.
- [18] R. Haldavnekar, K. Venkatakrishnan, and B. Tan, "Non plasmonic semiconductor quantum SERS probe as a pathway for *in vitro* cancer detection," *Nature Commun.*, vol. 9, no. 1, pp. 1–18, Dec. 2018, doi: 10.1038/s41467-018-05237-x.
- [19] M. C. C. G. Carneiro, A. Sousa-Castillo, M. A. Correa-Duarte, and M. G. F. Sales, "Dual biorecognition by combining molecularly-imprinted polymer and antibody in SERS detection. Application to carcinoembryonic antigen," *Biosensors Bioelectron.*, vol. 146, Dec. 2019, Art. no. 111761.
- [20] P. Kusch, S. Mastel, N. S. Mueller, N. Morquillas Azpiazua, S. Heeg, R. Gorbachev, F. Schedin, U. Hübner, J. I. Pascual, S. Reich, and R. Hillenbrand, "Dual-scattering near-field microscope for correlative nanoimaging of SERS and electromagnetic hotspots," *Nano Lett.*, vol. 17, no. 4, pp. 2667–2673, Apr. 2017.
- [21] A. R. L. Marshall, J. Stokes, F. N. Viscomi, J. E. Proctor, J. Gierschner, J.-S. G. Bouillard, and A. M. Adawi, "Determining molecular orientation via single molecule SERS in a plasmonic nano-gap," *Nanoscale*, vol. 9, no. 44, pp. 17415–17421, 2017.
- [22] T.-T. Pan, D.-W. Sun, J. Paliwal, H. Pu, and Q. Wei, "New method for accurate determination of polyphenol oxidase activity based on reduction in SERS intensity of catechol," *J. Agricult. Food Chem.*, vol. 66, no. 42, pp. 11180–11187, Oct. 2018, doi: 10.1021/acs.jafc.8b03985.
- [23] J. Guo, F. Zeng, J. Guo, and X. Ma, "Preparation and application of microfluidic SERS substrate: Challenges and future perspectives," *J. Mater. Sci. Technol.*, vol. 37, pp. 96–103, Jan. 2020, doi: 10.1016/j.jmst.2019.06.018.
- [24] L. Li, M. Liao, Y. Chen, B. Shan, and M. Li, "Surface-enhanced Raman spectroscopy (SERS) nanoprobe for ratiometric detection of cancer cells," *J. Mater. Chem. B*, vol. 7, no. 5, pp. 815–822, Jan. 2019, doi: 10.1039/C8TB02828A.
- [25] S. E. J. Bell, G. Charron, E. Cortés, J. Kneipp, M. L. de la Chapelle, J. Langer, M. Procházka, V. Tran, and S. Schlücker, "Towards reliable and quantitative surface-enhanced Raman scattering (SERS): From key parameters to good analytical practice," *Angew. Chem. Int. Ed.*, vol. 59, no. 14, pp. 5426–5454, 2020, doi: 10.1002/anie.201908154.
- [26] K. Kneipp, "Chemical contribution to SERS enhancement: An experimental study on a series of polymethine dyes on silver nanoaggregates," *J. Phys. Chem. C*, vol. 120, no. 37, pp. 21076–21081, Sep. 2016.
- [27] C. Zhou, L. Sun, F. Zhang, C. Gu, S. Zeng, T. Jiang, X. Shen, D. S. Ang, and J. Zhou, "Electrical tuning of the SERS enhancement by precise defect density control," *ACS Appl. Mater. Interfaces*, vol. 11, no. 37, pp. 34091–34099, Sep. 2019, doi: 10.1021/acsami.9b10856.
- [28] M. Zakia, H. Song, C. H. Song, S.-M. Jin, E. Lee, Y. S. Won, K. Kim, K.-S. Kim, J. Yoon, and S. I. Yoo, "Scattering-mediated absorption from heterogeneous nanoparticle assemblies in diblock copolymer micelles for SERS enhancement," *J. Mater. Chem. C*, vol. 7, no. 17, pp. 5051–5058, 2019.
- [29] P. A. Mercadal, E. R. Encina, J. E. L. Villa, and E. A. Coronado, "A new figure of merit to assess the SERS enhancement factor of colloidal gold nanoparticle aggregates," *J. Phys. Chem. C*, vol. 125, no. 7, pp. 4056–4065, Feb. 2021.
- [30] Z. Li and D. Kurouski, "Nanoscale structural characterization of plasmon-driven reactions," *Nanophotonics*, vol. 10, no. 6, pp. 1657–1673, Apr. 2021, doi: 10.1515/nanoph-2020-0647.
- [31] N. Banaei, A. Foley, J. M. Houghton, Y. Sun, and B. Kim, "Multiplex detection of pancreatic cancer biomarkers using a SERS-based immunoassay," *Nanotechnology*, vol. 28, no. 45, Nov. 2017, Art. no. 455101, doi: 10.1088/1361-6528/aa8e8c.
- [32] D. Graham et al., "Theory of SERS enhancement: General discussion," *Faraday Discuss.*, vol. 205, pp. 173–211, Nov. 2017.

- [33] L. Xie, J. Lu, T. Liu, G. Chen, G. Liu, B. Ren, and Z. Tian, "Key role of direct adsorption on SERS sensitivity: Synergistic effect among target, aggregating agent, and surface with Au or Ag colloid as surface-enhanced Raman spectroscopy substrate," *J. Phys. Chem. Lett.*, vol. 11, no. 3, pp. 1022–1029, 2020.
- [34] H. Wei, W. Leng, J. Song, M. R. Willner, L. C. Marr, W. Zhou, and P. J. Vikesland, "Improved quantitative SERS enabled by surface plasmon enhanced elastic light scattering," *Anal. Chem.*, vol. 90, no. 5, pp. 3227–3237, Mar. 2018, doi: [10.1021/acs.analchem.7b04667](https://doi.org/10.1021/acs.analchem.7b04667).
- [35] E. C. L. Ru and P. G. Etchegoin, "Single-molecule surface-enhanced Raman spectroscopy," *Annu. Rev. Phys. Chem.*, vol. 63, no. 1, pp. 65–87, May 2012, doi: [10.1146/annurev-physchem-032511-143757](https://doi.org/10.1146/annurev-physchem-032511-143757).
- [36] S. I. Maslovski and C. R. Simovski, "Purcell factor and local intensity enhancement in surface-enhanced Raman scattering," *Nanophotonics*, vol. 8, no. 3, pp. 429–434, Jan. 2019.
- [37] S. Kumar, K. Tokunaga, K. Namura, T. Fukuoka, and M. Suzuki, "Experimental evidence of a twofold electromagnetic enhancement mechanism of surface-enhanced Raman scattering," *J. Phys. Chem. C*, vol. 124, no. 38, pp. 21215–21222, Sep. 2020, doi: [10.1021/acs.jpcc.0c07930](https://doi.org/10.1021/acs.jpcc.0c07930).
- [38] E. C. L. Ru and P. G. Etchegoin, "Quantifying SERS enhancements," *MRS Bull.*, vol. 38, no. 8, pp. 631–640, Aug. 2013, doi: [10.1557/mrs.2013.158](https://doi.org/10.1557/mrs.2013.158).
- [39] R. J. Bartlett, "Adventures in DFT by a wavefunction theorist," *J. Chem. Phys.*, vol. 151, no. 16, pp. 1–19, 2019, doi: [10.1063/1.5116338](https://doi.org/10.1063/1.5116338).
- [40] S. Liu, X. Zhao, Y. Li, M. Chen, and M. Sun, "DFT study of adsorption site effect on surface-enhanced Raman scattering of neutral and charged pyridine-Ag₄ complexes," *Spectrochim. Acta A. Mol. Biomol. Spectrosc.*, vol. 73, no. 2, pp. 382–387, Jul. 2009, doi: [10.1016/j.saa.2009.02.036](https://doi.org/10.1016/j.saa.2009.02.036).
- [41] E. Solano-Ruiz, R. S. Berrú, J. Ocotlán-Flores, and J. M. Saniger, "Synthesis of silver nanoparticles by sonochemical induced reduction application in SERS," *J. Nano Res.*, vol. 9, pp. 77–81, Feb. 2010, doi: [10.4028/www.scientific.net/JNanoR.9.77](https://doi.org/10.4028/www.scientific.net/JNanoR.9.77).
- [42] C.-H. Zhang, J. Zhu, J.-J. Li, and J.-W. Zhao, "Small and sharp triangular silver nanoplates synthesized utilizing tiny triangular nuclei and their excellent SERS activity for selective detection of thiram residue in soil," *ACS Appl. Mater. Interfaces*, vol. 9, no. 20, pp. 17387–17398, May 2017, doi: [10.1021/acsami.7b04365](https://doi.org/10.1021/acsami.7b04365).
- [43] B. Wang, L. Zhang, and X. Zhou, "Synthesis of silver nanocubes as a SERS substrate for the determination of pesticide paraoxon and thiram," *Spectrochim. Acta A, Mol. Biomol. Spectrosc.*, vol. 121, pp. 63–99, 2014, doi: [10.1016/j.saa.2013.10.013](https://doi.org/10.1016/j.saa.2013.10.013).
- [44] D. Jana, A. Mandal, and G. De, "High Raman enhancing shape-tunable ag nanoplates in alumina: A reliable and efficient SERS technique," *ACS Appl. Mater. Interfaces*, vol. 4, no. 7, pp. 3330–3334, Jul. 2012, doi: [10.1021/am300781h](https://doi.org/10.1021/am300781h).



and received a national invention patent as the first inventor in China.

XU YANG was born in Jilin, China, in 1991. She received the bachelor's and master's degrees in safety engineering from Harbin University of Science and Technology, Harbin, China, in 2014 and 2016, respectively, where she is currently pursuing the Ph.D. degree in precision instruments and machinery. Her research interest includes surface-enhanced Raman scattering by metallic nanoparticles. She has published many papers in relevant international conference proceedings and journals



His research interests include system reliability engineering and detection technology, and he has published more than 20 articles as the corresponding author in relevant journals. He has served as a reviewer for some journals.

ZHEN ZHOU was born in Harbin, Heilongjiang, China, in 1960. He received the bachelor's degree in biology and medical instruments from the Department of Science and Experimental Instrument Engineering, Zhejiang University, in 1983, and the master's and Ph.D. degrees in measurement technology and instruments from Harbin University of Science and Technology, Harbin, in 1991 and 2005, respectively.



published many papers in relevant international conference proceedings and journals. She has served as a reviewer for some journals.

JIA QI was born in Harbin, Heilongjiang, China, in 1987. She received the bachelor's degree in engineering from Yantai University, Yantai, China, in 2010, and the master's degree in measurement technology and instruments and the Ph.D. degree in precision instruments and machinery from Harbin University of Science and Technology, Harbin, in 2014 and 2019, respectively. Her research interests include system reliability engineering and detection technology, and has published many papers in relevant international conference proceedings and journals.



international conference proceedings and journals. She has served as a reviewer for some journals.

SIQI ZHANG was born in Heilongjiang, China, in 1991. She received the bachelor's degree in safety engineering from Hebei University of Engineering, in 2013, and the master's degree in safety engineering and the Ph.D. degree in precision instrument and mechanical engineering from Harbin University of Science and Technology, in 2016 and 2021, respectively. Her research interest includes particle optical measurement technology, and has published many papers in relevant international conference proceedings and journals.



Since 2015, she has been a Lecturer with the Department of Safety Engineering, Harbin University of Science and Technology, China. She has authored one book, six articles, and three inventions. Her research interests include nonlinear dynamics and reliability of intelligent structures.

KANGKANG GUO was born in Handan, Hebei, China, in 1987. She received the Ph.D. degrees in general mechanics and fundamentals of mechanics from Tianjin University, in 2015.



Since 2015, he has been an Associate Professor with the Higher Educational Key Laboratory for Measuring and Control Technology and Instrumentations of Heilongjiang Province, Harbin University of Science and Technology, China. He has authored six articles and 18 inventions. He is interested in optical metrology using image processing and computational camera development.

...